1. Mariusz KLIMEK[1], 2. Adam KURNICKI[2]

ACCREA Medical Robotics Sp. z o.o. (1), Politechnika Lubelska (2)
ORCID: 1. 0009-0004-1490-6310; 2. 0000-0002-4988-7322

doi:10.15199/48.2024.03.24

Online Calibration of Strain Gauge Based Force/Torque Sensor used for simple interaction human - manipulator

Abstract. *The process of calibrating force-torque sensors with high precision is quite time-consuming and necessitates dismantling the system in which the sensor is utilized. This paper proposes method to calibrate six-axis, low-cost force-torque sensors that can be performed in situ and online i.e., without removing the sensor from the manipulator and directly by algorithm implemented on manipulator controller. This approach is validated by comparing the results obtained by calibrations carried out using the presented online method and the offline method utilizing a calibration jig.*

Streszczenie. *Skalowanie czujników siła-moment jest procesem czasochłonnym, wymagającym odmontowania czujnika od manipulatora. W artykule zaproponowano metodę skalowania sześcioosiowych, nisko kosztowych FTS, która jest wykonywana w czasie rzeczywistym, bez konieczności demontażu czujnika. Wyniki skalowania uzyskane za pomocą przedmiotowej metody zostały zweryfikowane na drodze porównania z wynikami skalowania zrealizowanymi metodą offline z wykorzystaniem specjalnego przyrządu kalibracyjnego.. (**Skalowanie online tensometrycznego czujnika siła/moment dedykowanego dla zastosowań do prostych interakcji człowiek-manipulator**).*

Słowa kluczowe: czujnik siła/moment, skalowanie online, metoda najmniejszych kwadratów, czujnik nisko kosztowy
Keywords: Force Torque Sensor, Online Calibration, Least Squares Method, Low-Cost sensor

Introduction

The six-axis Force Torque Sensor (FTS) exhibits the capacity to concurrently measure three axial forces (F_x, F_y, F_z) and torques (M_x, M_y, M_z) exerted upon it. This type of sensor is widely utilized across diverse fields, with a prominent presence in robotics. However, the acquisition of a highly accurate FTS entails a cost that proves excessively burdensome for numerous applications. Furthermore, certain applications do not require a high level of precision [1]. For instance, when executing tasks such as manually guiding the manipulator's end-effector or detecting external impacts experienced by the manipulator during human – robot interaction, a relative error of 10% is deemed permissible.

In general, the six-axis FTSs can be categorized into two types based on the relationship between applied force/torque and the resulting measuring bridges output signals values [2]: mechanically coupled sensors and mechanically decoupled sensors. Mechanically coupled sensors generate an output signal in multiple bridge circuits when a pure force/torque component is applied, requiring calibration using a complicated calibration matrix. On the other hand, mechanically decoupled sensors selectively respond in their bridge circuit output to specific force or torque components. Compared to mechanically coupled sensors, mechanically decoupled sensors offer easier sensor calibration and maintenance since their output signals are physically decoupled.

The mechanical decoupling strategy is followed by many researchers as described, e.g. in [2-5]. A new structure of a sensing element and placement of strain gauges is proposed in [2-4]. In [5] a Finite Element Method (FEM) is used to evaluate the coupling terms and minimize them by changing geometric parameters of the underlying Computer Aided Design (CAD) model. In a different context, FEM is used to analyze stress-strain relations in [6]. In [1] the authors point that mechanical decoupling, i.e. modifying the mechanical construction of the sensor and strain gauges' placement, can lead to satisfactory results. However, production of sophisticated shapes of a sensing element can be expensive. Therefore, it is more economical to apply software decoupling. Software decoupling strategies vary from simple models, such as linear Least Squares Method (LSM), to more advanced nonlinear ones, like Support Vector Machines [7] and Neural Networks (NNs) [8]. In [8] authors claim that the nonlinear model based on NNs performs better as LSM. However, while NNs can be trained offline, they are infeasible for online calibration. The LSM is applied in [9] for the in situ calibration, i.e. decoupling.

This article presents an online, in-situ method used for calibration of cost-effective six-axis force-torque sensor. The FTS, which incorporates the Maltese cross design, plays a crucial role as an integral component within the Robot Interaction Module (RIM), which is utilized in human-robot interaction applications. Our approach does not require any usage of a dynamical model of the manipulator. This method, addressing the needs of regular calibration [9], particularly offset removal, just before using FTS, can be conducted without the necessity of disassembling the sensor from the manipulator. Its implementation can utilize a standard manipulator controller without the need to collect and process a large amount of experimental measurement data beforehand. The calibration outcomes achieved through this approach are compared to those obtained using the classical method that relies on conducting offline measurement experiments with a specialized calibration jig. While the latter technique offers higher accuracy, it is more time-consuming and necessitates the disassembly of the FTS sensor, its repeated assembly (in various configurations) on the calibration jig, and the collection and resource-intensive processing of measurement data.

Sensor structure and strain gauges arrangement

The force/torque sensor, whose calibration is the subject of this article is the main component of the robot interactive module. The structure of the RIM is shown in Fig. 1(a), while the mechanical structure of the FTS itself is depicted in Fig. 1(b). The sensor is constructed as a modified Maltese cross made of aluminum alloy. It consists of an outer ring and a hexahedral hub connected by four elastic beams. Loads are applied to the sensor through an end-effector adapter attached to the hub. The outer ring is firmly fixed to the manipulator wrist via a mounting flange. In order to enhance sensitivity of horizontal lateral forces F_y and F_z the connection between cross elastic beam and the outer ring is equipped with additional compliant beams (see Fig. 1 (b)). On the opposite sides of the cross beams, pairs of strain gauges are attached, forming 8 half Wheatstone bridges. The sensor coordinate system was selected such

that the *X*-axis is orthogonal to the sensor's plane, while the *Y* and *Z* axes align with the symmetry axes of the cross beams.

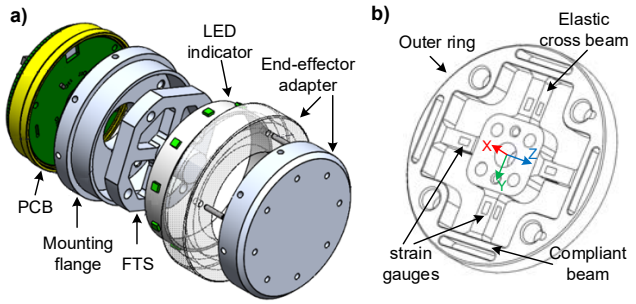

Fig. 1. Robot interaction module structure (a) RIM assembly (b) FTS structure and coordinates

The simplified measurement system, employed for acquiring measurement signals from the strain gauge half-bridges, is depicted in Fig. 2. This system (with exception of strain gauges) is implemented in the printed circuit board (PCB) mounted alongside the FTS sensor (see Fig. 1(a)).

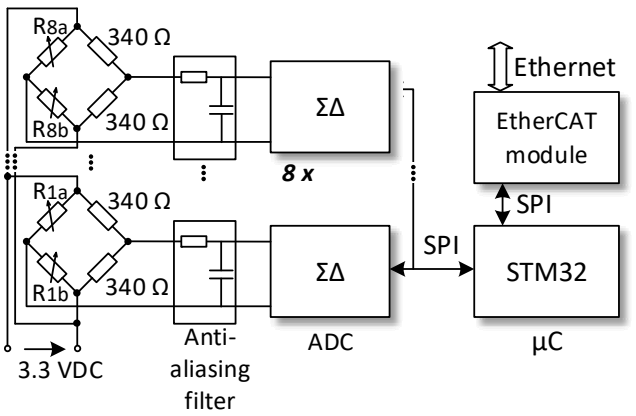

Fig. 2. FTS measurement circuit

The output (unbalanced) voltage from each of the bridges shown in Fig. 2 is first filtered by an RC anti-aliasing filter, then amplified 128 times, converted to a 24-bit digital signal and further filtered by the digital filter of a ΣΔ analog to digital converter (ADC). Subsequently, these signals are transmitted at a rate of 1 kHz to the STM32 microcontroller, where they undergo validation and additional conditioning, including offset removal upon request. The signals are then transformed into forces and torques by multiplying their values with the calibration matrix. The calculated measurement values are then transmitted to the master controller of the manipulator via Ethernet.

Mathematical model of the sensor

The mathematical model which represents the calculation of force-torque (also called wrench *W*) measurement values based on bridge strain measurements $\Delta \in R^8$, assuming linear sensors and the absence of initial strains (offsets):

(1) $$W = C\Delta$$

where: $C \in R^{6\times 8}$ is strain stiffness matrix (calibration matrix), $W \in R^6$ is wrench vector, composed of force $\vec{F}$ and torque $\vec{M}$ vectors:

(2) $$W = \left[\vec{F}, \vec{M}\right]^T = \left[F_x, F_y, F_z, M_x, M_y, M_z\right]^T$$

In practical applications, it is not valid to assume that strains are zero when no wrench is applied to the sensor. Therefore, it becomes necessary to incorporate a strain offset $D_\Delta \in R^8$ into the model:

(3) $$W = C(\Delta + D_\Delta) = C\Delta + CD_\Delta = C\Delta + D$$

where: $D \in R^6$ is wrench offset vector.

It is assumed that the elements of the calibration matrix and the offset vector remain constant.

Determination of the Calibration Matrix

In order to implement equations (1) or (3), which involve calculating forces and torques from measured strains, it is essential to possess information about the calibration matrix C. The derivation of this matrix involves solving an overdetermined system of equations:

(4) $$\tilde{W} = C\tilde{\Delta},$$

utilizing known values of *n* strain vectors *Δ* ($\tilde{\Delta} = \left[\Delta_1, \Delta_2, \ldots, \Delta_n\right] \in R^{8\times n}$) and *n* vectors *W* of forces and torques that are applied to the sensor ($\tilde{W} = \left[W_1, W_2, \ldots, W_n\right] \in R^{6\times n}$). The estimation of the matrix C's elements is accomplished through the ordinary least squares method.

Matrix *C* consists of six rows, and each row consists of eight coefficients that represents the degree of dependence between the calculated values F_x, F_y, F_z, M_x, M_y, M_z and the individual values of the strain measurement vector $\Delta = \left[\Delta^1, \Delta^2, \ldots, \Delta^k, \ldots, \Delta^8\right]^T$. To achieve a proper estimation of these eight coefficients (obtain an unambiguous solution) it is essential to have a minimum of eight linearly independent equations. However, in this case, the given set of equations (4) can only provide a maximum of six linearly independent equations. Therefore, additional information regarding the arrangement of measurement bridges and the coordinate system relative to the sensor (see Fig. 1(b)) was utilized. Consequently, under the assumption of an ideally manufactured sensor, the relationship (1) between the vector *W* and the strain *Δ* is expressed as follows:

(5) $$W = \overline{C}\begin{bmatrix} -\Delta^2 - \Delta^4 - \Delta^6 - \Delta^8 \\ \Delta^3 - \Delta^7 \\ \Delta^1 - \Delta^5 \\ \Delta^1 + \Delta^3 + \Delta^5 + \Delta^7 \\ -\Delta^4 + \Delta^8 \\ -\Delta^2 + \Delta^6 \end{bmatrix} = \overline{C}\overline{\Delta} = \overline{C}P\Delta$$

where: $\overline{C} \in R^{6\times 6}$ is a modified calibration matrix, $\overline{\Delta} \in R^6$ is modified (projected) strain vector, $P \in R^{8\times 6}$ is a projection matrix:

(6) $$P=\begin{bmatrix} 0 & -1 & 0 & -1 & 0 & -1 & 0 & -1 \\ 0 & 0 & +1 & 0 & 0 & 0 & -1 & 0 \\ +1 & 0 & 0 & 0 & -1 & 0 & 0 & 0 \\ +1 & 0 & +1 & 0 & +1 & 0 & +1 & 0 \\ 0 & 0 & 0 & -1 & 0 & 0 & 0 & +1 \\ 0 & -1 & 0 & 0 & 0 & +1 & 0 & 0 \end{bmatrix}.$$

If an ideal sensor is considered, the matrix $\overline{C}$ will take the form of a diagonal matrix, where the coefficients represent the scaling of strains $\overline{\Delta}$ into subsequent forces and torques. However, for a real sensor, the matrix $\overline{C}$ deviates from being diagonal. Then by multiplying this non-diagonal matrix by the projection matrix *P*, the desired calibration matrix *C* is obtained:

(7) $$C=\overline{C}P.$$

Online Ordinary Least Squares Method

In order to create an algorithm that determines the matrix *C* online, first the relation (4) should be multiplied by the Moore-Penrose right-pseudoinverse of $\tilde{\Delta}$, which is defined as follows:

(8) $$\tilde{\Delta}^{\#}=\tilde{\Delta}^{T}\left(\tilde{\Delta}\tilde{\Delta}^{T}\right)^{-1}$$

Since $\tilde{\Delta}\tilde{\Delta}^{\#}=I$, the solution for *C* is then given by:

(9) $$C=\tilde{W}\tilde{\Delta}^{\#}=\tilde{W}\tilde{\Delta}^{T}\left(\tilde{\Delta}\tilde{\Delta}^{T}\right)^{-1}.$$

In the equation (9) the *(j,k)*-th component of $\tilde{W}\tilde{\Delta}^{T}$ can be represented by:

(10) $$\left(\tilde{W}\tilde{\Delta}^{T}\right)_{j,k}=\sum_{i=1}^{n}(W_i)_j(\Delta_i)_k=\left(\sum_{i=1}^{n}W_i\Delta_i^{T}\right)_{j,k}$$

and the *(j,k)*-th component of $\tilde{\Delta}\tilde{\Delta}^{T}$ by:

(11) $$\left(\tilde{\Delta}\tilde{\Delta}^{T}\right)_{j,k}=\sum_{i=1}^{n}(\Delta_i)_j(\Delta_i)_k=\left(\sum_{i=1}^{n}\Delta_i\Delta_i^{T}\right)_{j,k},$$

where: *i* is an index representing the column number of the matrix $\tilde{\Delta}$ and $\tilde{W}$. Then the closed form of solution (9) used in online method is as follows:

(12) $$C=\left[\sum_{i=1}^{n}W_i\Delta_i^{T}\right]\left[\sum_{i=1}^{n}\Delta_i\Delta_i^{T}\right]^{-1}=S_{W\Delta}\left(S_{\Delta\Delta}\right)^{-1}.$$

In order to achieve a successful calculation of matrix *C* using either formula (12) or (9), it is essential that matrix $\tilde{\Delta}\tilde{\Delta}^{T}$ is invertible, meaning that $\tilde{\Delta}$ should possess independent rows. Therefore, using relation (12), a modified calibration matrix $\overline{C}$ is calculated (instead of matrix *C*) as a result of replacing the strain vector Δ by the projected strain vector $\overline{\Delta}$.

The developed method must be able to determine, in addition to the matrix C, the wrench offset vector *D*. Therefore, in formula (12), instead of the projected strain vector $\overline{\Delta}$, a vector appended by a unit element is introduced as input:

(13) $$\overline{\Delta}^{*}=\left[\overline{\Delta}^{T},1\right]^{T},$$

and then instead of $\overline{C}$ an augmented calibration matrix:

(14) $$\overline{C}^{*}=\left[\overline{C},D\right]$$

is calculated.

The determination of the matrix *C* according to relation (12) can be implemented using an iterative method. Then, at the beginning, the matrices $S_{W\Delta}$ and $S_{\Delta\Delta}$ are zero matrices and then, in successive iterations (i.e. for the following pairs of vectors W_i and Δ_i), they are calculated as follows:

(15) $$S_{W\Delta}:=S_{W\Delta}+W_i\Delta_i^{T},$$

(16) $$S_{\Delta\Delta}:=S_{\Delta\Delta}+\Delta_i\Delta_i^{T}.$$

After the end of the *n*-th iteration, the matrix *C* is calculated according to the right side of relation (12).

In Situ Online Calibration Method

Due to the non-ideal nature of the FTS, characterized by factors like non-linearities and stress changes due to temperature variations, the least square method for determining the *C*-matrix will be more effective with a larger number *n* of input data points and a more uniform distribution of these data points across the sensor's measurement range. These data points, represented as pairs of W_i and Δ_i vectors, are obtained through experiments where the sensor is subjected to known loads. To achieve on-line calibration, the proposed in situ method can be utilized. This calibration method can be performed on demand without the need for additional measuring and control equipment. The approach employs a standard manipulator equipped with a RIM (FTS) and a specialized RIM calibration tool (RCT) mounted as the manipulator's end-effector (refer to Fig. 3).

During the course of the experiment, the end-effector undergoes changes in its orientation relative to the ground. Cyclic calculations are then carried out using equations (15) and (16). The Δ_i values represent the direct outcomes of strain measurements, while the components of the vector W_i, comprising force vector $\vec{F}_i$ and torques, are calculated as follows:

(17) $$\vec{F}_i=R_i m_0\vec{g},,$$

(18) $$\vec{M}_i=\vec{r}_0\times\vec{F}_i$$

using information about the known mass m_0 and center of gravity $\vec{r}_0$ of the RCT, along with the known orientation R_i of the sensor coordinate system.

In order to uniquely define matrix *C* in equation (4), matrices Δ and *W* must be linearly independent. This requirement implies that matrix *W* needs to be full-rank, which means it must have a rank of 6. When considering a constant value of $\vec{r}_0$ and different orientations R_i, all torques calculated using relation (18) are subject to two additional equations:

(19) $$\vec{M}_i\cdot\vec{r}_0=(\vec{r}_0\times\vec{F}_i)\cdot\vec{F}_i=0,$$

(20) $$\vec{M}_i \cdot \vec{F}_i = (\vec{r}_0 \times \vec{F}_i) \cdot \vec{F} = 0$$

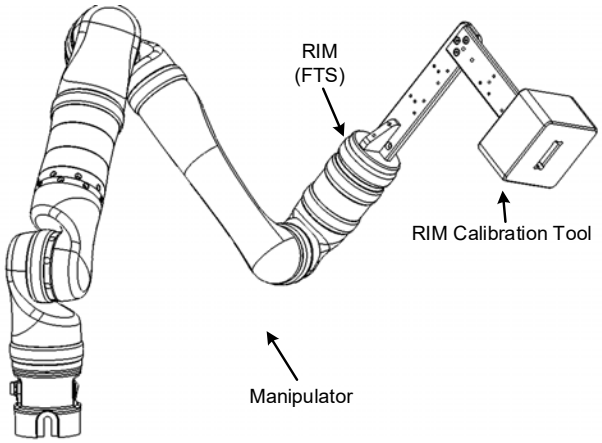

Fig. 3. Manipulator with RIM and RIM Calibration Tool

Then the knowledge of the 4 components of the vector W_i allows the calculation of the remaining 2. This applies to all W_i. However, due to this relationship, the matrix $\tilde{W}$ ends up having only 4 linearly independent rows instead of the required 6, leading to its rank being 4. The number of linearly independent rows in matrix $\tilde{W}$ can be increased by conducting experiments with another value of $\vec{r}_0$, appearing in equations (18) and (19).

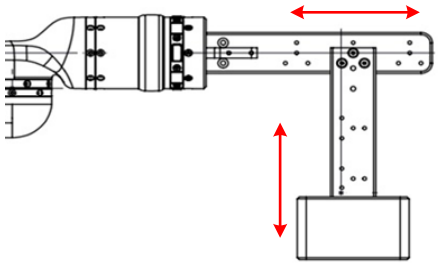

Fig. 4. RIM Calibration Tool reconfiguration possibilities

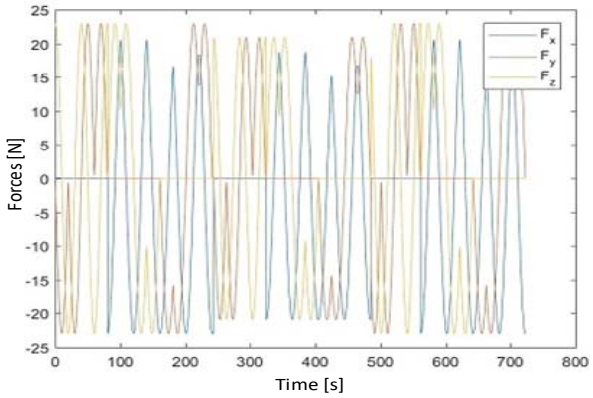

Fig.5. Forces acting on FTS

In summary, to achieve a full-rank $\tilde{W}$ matrix, it is essential to employ at least three different values $\vec{r}_1$, $\vec{r}_2$, $\vec{r}_3$ (instead of a single $\vec{r}_0$), representing the center of mass of the RCT during the calibration experiment.

In the arrangement shown in Fig. 3, all that is needed to properly perform the calibration experiment is to vary the angular positions in the range of +/- 180° for the last two joints in an appropriate manner. This should be done sequentially for the three configurations (i.e. three different centers of mass) of the RCT. The RCT allows the configuration to be changed by moving the main weight in two directions as shown in Fig. 4.

The forces and torques waveforms acting on the FTS, used during the calibration experiment, are shown in Fig. 5 and 6 respectively.

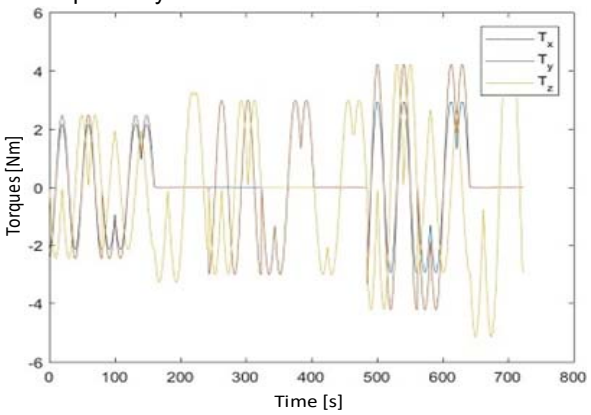

Fig.6. Torques acting on FTS

Simulation validation of the method

The developed method was initially validated through simulation. This validation process involved applying the calibration procedure to a series of input data W_i and $\overline{\Delta}_i$. These data were not obtained from actual experiments but were instead calculated based on the FTS mathematical model derived from equations (3) and (5):

(21) $$W_i = \overline{C} \cdot \overline{\Delta}_i + D$$

To generate the data, arbitrary assumptions about the modified calibration matrix $\overline{C}$ and the wrench offset vector D were made. Then, successive vectors $\overline{\Delta}_i$ were calculated, using the relation resulting from the transformation of equation (21):

(22) $$\overline{\Delta}_i = \overline{C}^{-1}(W_i - D).$$

Next, the resulting calibration matrix was compared with the one used for the data generation. The comparison results for the $\overline{C}_{11}$ element of the calibration matrix in each iteration of the algorithm are presented in Fig. 7.

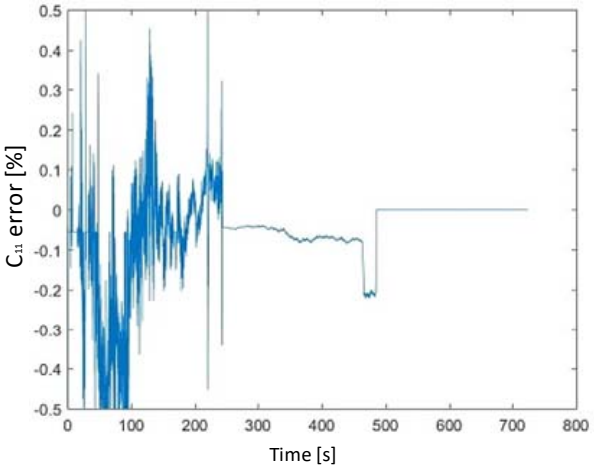

Fig 7. Relative error in the determination of the coefficient $\overline{C}_{1,1}$ of the calibration matrix

The error waveform exhibits a noticeable trend of approaching zero for the $\overline{C}_{11}$ error value with an increase in the algorithm iterations. This convergence can be observed in three distinct intervals, each showing an abrupt decrease in the error value. These changes are directly associated with consecutive alterations in the center of mass of the RCT. It is noteworthy that the data originating from the third RCT configuration leads to a minimized $\overline{C}_{11}$ determination error, effectively reaching zero. A comparable pattern of convergence for the error was also observed for the other coefficients of the $\overline{C}$ matrix, as well as for the *D* vector.

The results of the simulation validation experiments confirmed the correctness of the developed method

Experimental validation of the method

The validation process under real calibration experiment conditions carried out on a physical sensor was conducted in multiple stages. In the first stage, offline input data were collected using a dedicated calibration jig (see Fig. 8). On this device, pure axial forces and torques acting on the sensor were generated by appropriately mounting the FTS on jig and suspending weights on cables. Each force and torque was applied stepwise by dividing the whole sensor nominal load range (+/- 50 N and +/- 5 Nm) into 10 increments creating matrix $\tilde{W}$. Simultaneously, strain measurements were obtained, and after offset removal, they constituted matrix $\tilde{\Delta}$. Then, by multiplying matrix $\tilde{\Delta}$ by the projection matrix *P* and using successively relations (9) and (7), the calibration matrix *C* shown in Table 1 was determined. Almost identical values of the coefficients of matrix *C* were obtained using relations (15), (16) and (12) utilized in online calibration method.

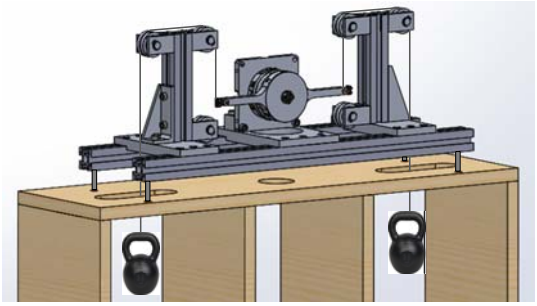

Fig.8. FTS calibration using calibration jig

In the second stage, the in situ online calibration method described in the previous chapter was used to determine the *C* matrix. The resulting calibration matrix is presented in Table 2.

During the final stage, a comparison was made between the results obtained in the first two stages by calculating the forces and moments by multiplying the measured strains by both the matrix in Table 1 and Table 2. This experiment was done in a system with a manipulator (see Fig. 3) moving the arm end-effector in a way that produced different forces and moments acting on the FTS than those used during the calibration experiment. The waveform of the force acting in the x-axis direction is shown in Fig. 9. The waveform of the measurement error, calculated as the difference between the value of the acting force F_x and the value of this force determined using the matrix from Table 2, is shown in Fig. 10. A similar waveform of the error was obtained comparing the forces determined using both methods, i.e. using the matrices from Tables 1 and 2. On this basis, it can be concluded that the measurement error of the force F_x is less than 10%. In reality, the value of this error is expected to be lower, as its higher value is caused by the uncompensated dynamics in the system accompanying the arm movement. For torques and forces acting in other directions, the value of the measurement error is even slightly smaller.

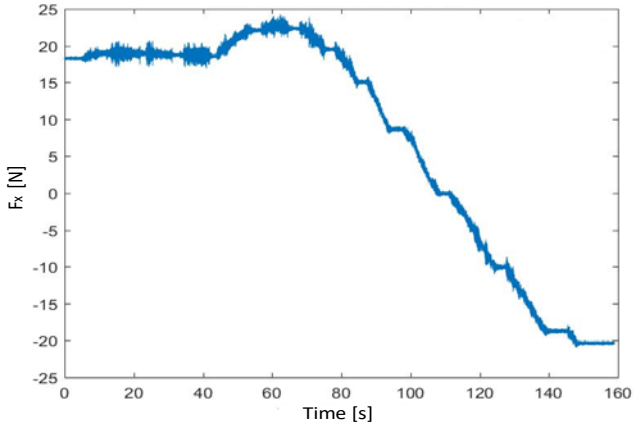

Fig 9. Force F_x acting on FTS during validation experiment

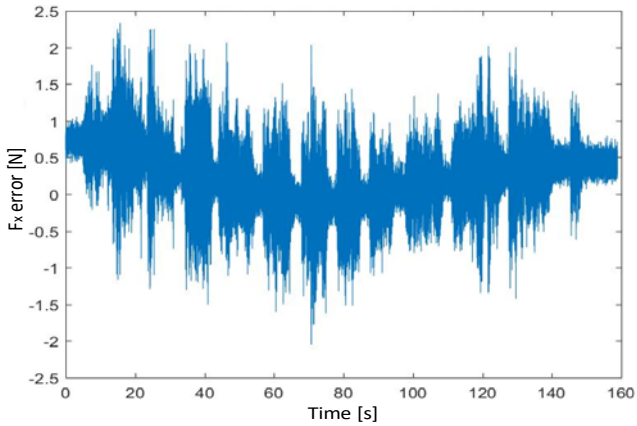

Fig 10. Absolute error of force F_x measurement during validation experiment

Table 1. Calibration matrix obtained using offline measurements

	Δ^1	Δ^2	Δ^3	Δ^4	Δ^5	Δ^6	Δ^7	Δ^8
Fx	-0.0783	115.9959	0.9697	116.2178	1.3307	115.8044	0.2828	115.5825
Fy	-261.2932	0.4277	-0.7689	-1.1942	260.2123	-2.8367	-0.3119	-1.2148
Fz	-1.8840	-1.9708	-268.3156	-0.5501	-2.5808	2.0404	263.8509	0.6196
Mx	2.8420	-0.0162	2.8130	-0.0295	2.7539	-0.0427	2.7829	-0.0294
My	0.1194	2.7478	0.0584	0.0326	-0.1015	-2.7470	-0.0405	-0.0318
Mz	-0.0495	-0.0221	0.0971	2.7913	0.0981	0.0448	-0.0485	-2.7686

Table 2. Calibration matrix obtained using in situ online method

	Δ^1	Δ^2	Δ^3	Δ^4	Δ^5	Δ^6	Δ^7	Δ^8
Fx	3.0923	115.3273	4.7326	115.7136	-2.1440	115.6176	-3.7843	115.2313
Fy	-259.3593	0.4145	14.1101	-0.3564	258.7215	-1.6980	-14.7478	-0.9271
Fz	-7.7659	-2.8778	-263.0028	-1.2387	3.2590	1.7686	258.4959	0.1295
Mx	3.4190	-0.2087	3.1167	-0.1291	2.0776	-0.1821	2.3799	-0.2618
My	-0.6157	2.7617	0.9176	-0.0135	0.5943	-2.5584	-0.9390	0.2169
Mz	-0.1800	0.2929	-0.1008	2.9374	0.1539	0.1548	0.0747	-2.4897

Conclusion

The development of a non-disassembly calibration method for force-torque sensors represents a significant advancement in robotics. This method effectively addresses the crucial need for frequent calibration, particularly offset removal, without necessitating sensor disassembly. The developed technique offers a streamlined and highly efficient approach, enabling users to maintain the accuracy of their FTS sensors without prolonged interruptions to the robot's operation. Furthermore, this calibration method does not demand any additional hardware or human resources, making it readily applicable in various robotic systems. It can be implemented on a simple microprocessor-based manipulator controller, without requiring significant memory resources and computing power.

Validation experiments carried out on the developed calibration method confirmed its correctness. The measured forces and torques have exhibited a level of precision sufficient for basic human-manipulator interactions, such as hand-guided movements or overload detection.

However, to further enhance measurement accuracy, there are potential approaches. One method involves compensating for the influence of arm dynamics during the calibration process, which unfortunately would require additional computing power. Alternatively, considering the values of measured strains in static arm positions for calculations could minimize measurement errors, but this approach would result in a significant increase in calibration time.

Acknowledgment

The authors would like to acknowledge the support of the National Centre for Research and Development as part of the "Smart Growth 2014-2020" project (activity 1.1), cofinanced by the European Regional Development Fund, for their funding of the L2R project, which provided the framework for the work presented in this article

***Authors**: dr inż. Mariusz Klimek, ACCREA Medical Robotics sp. z o.o., ul. Hiacyntowa 20, 20-143 Lublin, E-mail: m.klimek@accrea.com; dr inż. Adam Kurnicki,* Department of Automation and Metrology, Electrical Engineering and Computer Science Faculty, Lublin University of Technology, ul. Nadbystrzycka 38 A, 20-618 Lublin, *E-mail: a.kurnicki@pollub.pl.*

REFERENCES

[1] Song A. and Fu L., Multi-dimensional force sensor for haptic interaction: a review, *Virtual Reality and Intelligent Hardware*, 1 (2019), no. 2, 121– 135

[2] Sun Y., Liu Y., Zou T., Jin M., and Liu H., Design and optimization of a novel six-axis force/torque sensor for space robot, *Measurement*, 65 (2015), 135–148

[3] Hu S., Wang H., Wang Y., and Liu Z., Design of a novel six-axis wrist force sensor, *Sensors*, 18 (2018), no. 9

[4] Kebede G. A., Ahmad A. R., Lee S.-C., and Lin C.-Y., Decoupled six-axis force–moment sensor with a novel strain gauge arrangement and error reduction techniques, *Sensors*, 19 (2019), no. 13

[5] Kang M.-K., Lee S., and Kim J.-H., Shape optimization of a mechanically decoupled six-axis force/torque sensor, *Sensors and Actuators A: Physical*, 209 (2014), 41–51

[6] Khayrnasov K., Modeling and analysis of the stress-strain state of robotic systems, *Przegląd Elektrotechniczny*, 97 (2021), no. 8, 66-69

[7] Ma Y., Xie S., Zhang X., and Luo Y., Hybrid calibration method for six-component force/torque transducers of wind tunnel balance based on support vector machines, *Chinese Journal of Aeronautics*, 26 (2013), no. 3, 554–562

[8] Liang Q., Wu W., Coppola G., Zhang D., Sun W., Ge Y., and Wang Y., Calibration and decoupling of multi-axis robotic force/moment sensors, *Robotics and Computer-Integrated Manufacturing*, 49 (2018), 301–308

[9] Andrade Chavez F.J., Traversaro S. and Pucci D., Six-Axis Force Torque Sensor Model-Based In Situ Calibration Method and Its Impact in Floating-Based Robot Dynamic Performance, *Sensors,* 19 (2019), no. 24, 5521